Two-Neutron Correlations in the Photofission of Actinides

phd Thesis

Jeffrey S. Burggraf

January 19, 2018

Advisors: Prof. Dr. D. S. Dale

Department of Physics, Idaho State University

Abstract

Past study of fission reactions has established that fission neutrons are predominantly emitted by the fully accelerated fission fragments, as opposed to being emitted during scission. The velocities of the two fully accelerated fission fragments is of similar magnitude to the velocities of the fission neutrons as they are emitted in the fragment's rest frame. Thus, the motion of the fragments has a large effect on the kinematics of fission neutrons. This can be seen in the opening angle distributions of correlated neutron pairs from individual fission events. This effect has been measured multiple times for the spontaneous fission of ^{252}Cf and the thermal induced fission of ^{235}U with relatively good agreement. A primary motivation for this work is that to date there have been no reported measurements of this type with photofission. A project has been completed at the Idaho Accelerator Center to measure two-neutron correlations in photofission using bremsstrahlung photons produced via a low duty factor linear electron accelerator. The bremsstrahlung photons impinge upon an actinide target that is surrounded by a large neutron scintillation detector array capable of measuring particle position and time of flight, enabling the calculation of two-neutron opening angle and neutron energy. Correlated distributions in two-neutron opening angle, the angle between a neutron and the incident photon beam, and neutron energy are extracted from the data.

Contents

Chapter 1

Introduction

1.1 Physics of Nuclear Photofission

Photofission occurs during the de-excitation of a nucleus after the absorption of a photon. For photon energies between 6 and 25 MeV, this absorption occurs primarily through the giant dipole resonance (GDR). One distinct and useful aspect of photofission, particularly when compared to neutron-induced fission, is the simple set of selection rules for the transfer of angular momentum. In photofission, there is a relatively low transfer of angular momentum to the nucleus, and as a result photon absorption occurs primarily via E1 absorption and to a lesser extent E2 absorption. This restricts J^{π} values for even-even nuclei to 1^{+} and 1^{-}, and gives rise to anisotropies in the fission fragment angular distribution that are far more pronounced than they are for other types of fission. For this reason, photofission is commonly used as a means to study sub-nuclear structures and the fundamentals of the fission process.

1.1.1 Neutrons from Photofission

Neutron emission can be classified into two categories: delayed and prompt. Delayed neutrons account for only $\sim 1\%$ of total neutron emission in actinide

photofission [3]. Delayed neutrons are not important to this study, since this measurement is insensitive to them. Prompt neutrons are defined as neutrons that are emitted either immediately after ($< 10^{-14}$ seconds), or during the scission of the nucleus, and account for the remaining $\sim$ 99% of neutron emission [3]. Prompt neutron production is known to occur by means of two distinct mechanisms, the dominant of which is neutron emission from the fully accelerated fragments. The second mechanism, referred to as *early neutron* emission, is the emission of neutrons during either the scission of the nucleus or the acceleration of the fission fragments. Both cases are discussed below.

A large number of past studies have established that the majority of prompt fission neutrons (80%–98%) are emitted from the fully accelerated fragments [7], while the remaining 2%–20% percent are early neutrons. The nature of early neutrons has remained elusive ever since their first observation in 1962 by Bowman et al. [1]. Models of prompt neutron emission are based mainly on observations of neutron angular distributions relative to the fission axis–the axis along which the fragments travel in the center of momentum frame. Another observational input for prompt neutron modeling is the neutron-neutron (n-n) opening angle distribution of correlated neutron pairs. Because fission neutrons are predominantly emitted from the fully accelerated fragments, the distribution of n-n opening angles is highly reflective of the underlying fundamental fission kinematics.

There are, on average, about 2 or 3 neutrons released per fission. It has been shown that neutrons that are released from the fully accelerated fission fragments are evaporated isotropically in the fragment's rest frame, in which they are emitted at speeds comparable to that of the fragments themselves [10]. Thus, a significant portion of the kinetic energy of these neutrons comes from

the transnational motion of the fission fragments from which they are emitted. This leads to a characteristic distribution in the opening angles between pairs of neutrons, given that the neutrons came from the same fission event. To gain a qualitative understanding of the distribution, consider a pair of neutrons that are emitted from different fragments, which are moving in opposite directions. The boost that each neutron receives from the fragments will cause a tendency for the neutrons to travel in opposite directions. Because of this, the opening angle between them is more likely to be large, or close to 180°. Conversely, if two neutrons are emitted from the same fragment, they are both boosted in the same direction, which will tend to push them toward parallel trajectories. In this case, opening angles close to 0° are favored. The favoring of both small and large opening angles gives rise to a U-shaped distribution, where a minimum occurs near 90°.

A key feature of the two-neutron opening angle distribution is its dependence on neutron energy. As neutron energy increases, the characteristic U-shape of the opening angle distribution is expected to become stronger. In other words, there is a decrease in the rate of opening angles near the center of the distribution (at 90°) relative to the rates at 0° and 180°. This relationship is a direct consequence of the boost that the fission fragments provide to emitted neutrons. Fragments with the highest total kinetic energy give the largest boost to emitted neutrons. This, in turn, also intensifies the favoring of opening angles near 0° and 180°.

Scission neutrons

Scission neutrons are neutrons that are emitted before the rupture of the nucleus. The time between rupture and the emission of prompt neutrons is on

the order of 10^{-14} seconds, so timing cannot be used to distinguish prompt from scission neutrons. The existence of scission neutrons was first postulated by [1] in 1962, in order to explain a discrepancy between a neutron emission model, which was accepted at the time, and their measured angular distribution of prompt neutrons from the spontaneous fission of ^{252}Cf. By measuring the velocities of both fission fragments and a neutron–in 3-fold coincidence– the authors of [1] concluded that there must exist a small portion (10-15%) of emitted neutrons, dubbed scission neutrons, that are emitted isotropically in the lab frame before before scission. In the mid-late 1980s, this experiment was repeated by [11] and [2], who found that the number of scission neutrons is below 5% and 10%, respectively. In 2000, the authors of [6] claimed to have found errors in [1],[2], and [11], and that all three results reach an agreement of a 10% scission component after corrections for energy-resolution, timing, and neutron scattering from objects nearby the fission source. Most recently, [12] developed a "three-component" neutron emission model that accurately predicts the measured spectrum of gamma and neutron emission from ^{252}Cf. This model suggested a scission neutron component of $<$2%.

Scission neutrons are thought to be emitted isotropically in the lab frame, and so they have the effect of flattening out the "U"-shaped opening angle distribution. Because of this connection between neutron opening angle distributions and scission neutrons, opening angle measurements add to the growing breadth of nuclear data that is needed to shed light on the elusive scission neutrons, the understanding of which remains an open problem in nuclear physics.

1.2 Previous work

The first measurement of angular correlation among coincident neutrons from fission was performed by Debenedetti et al. [4] in 1948 using neutrons from the neutron induced fission of ^{235}U. It was already known at the time that fission neutrons are preferentially emitted in the same direction as the fission fragments. Because of this, in reference [4] it was hypothesised that there are measurable correlations between fission neutrons. This hypothesis was confirmed when they found that neutrons tend to be emitted preferentially at large opening angles. The next measurement of this type was performed nearly 30 years later by Pringle and Brooks in 1975 [9], in which neutrons emitted from the spontaneous fission (SF) of ^{252}Cf were found to have high coincidence rates at small opening angles near 0°, and at large opening angles near 180°. In order to remove the effects of detector geometry and efficiencies, reference [9] divided a correlated opening angle distribution by an uncorrelated opening angle distribution, which is similar to a technique used in this work. To date, numerous measurements of n-n angular correlation using ^{252}Cf have been performed (see works [9] [5] [8]). This makes ^{252}Cf a good benchmark for n-n angular correlation measurements. Other correlated n-n measurements have been performed using induced thermal induced fission of ^{235}U, ^{233}U, and ^{239}Pu [13]. This study is the first to report this type of measurement using neutrons from photofission.

Chapter 2

Methods

2.1 Experimental Apparatus

The experiment was carried out at the Idaho Accelerator Center, using their short pulsed linear accelerator. The accelerator is a radio frequency accelerator operating at the L–band frequency of 1300 MHz. It is capable of pulse widths ranging from 50 ps to 2 μs with a maximum energy of 44 MeV.

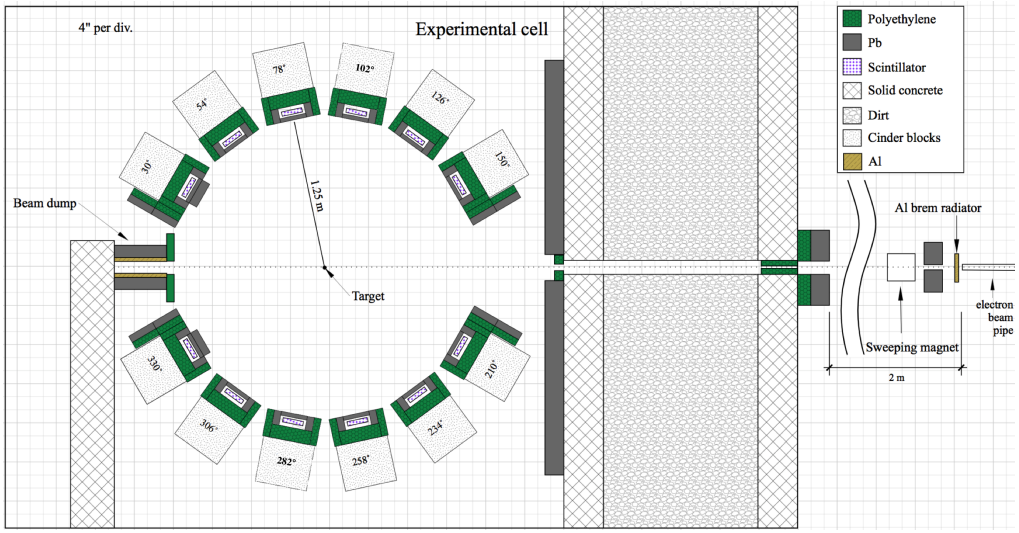

Figure 2.1: To-scale top down schematic of the entire experimental setup. The detectors supporting structures are each labeled with a degree value. The degree corresponds to the angle of the detector from the direction of the beam. For a better perspective of the scintillation cells alone, see 2.2

2.1.1 Detectors

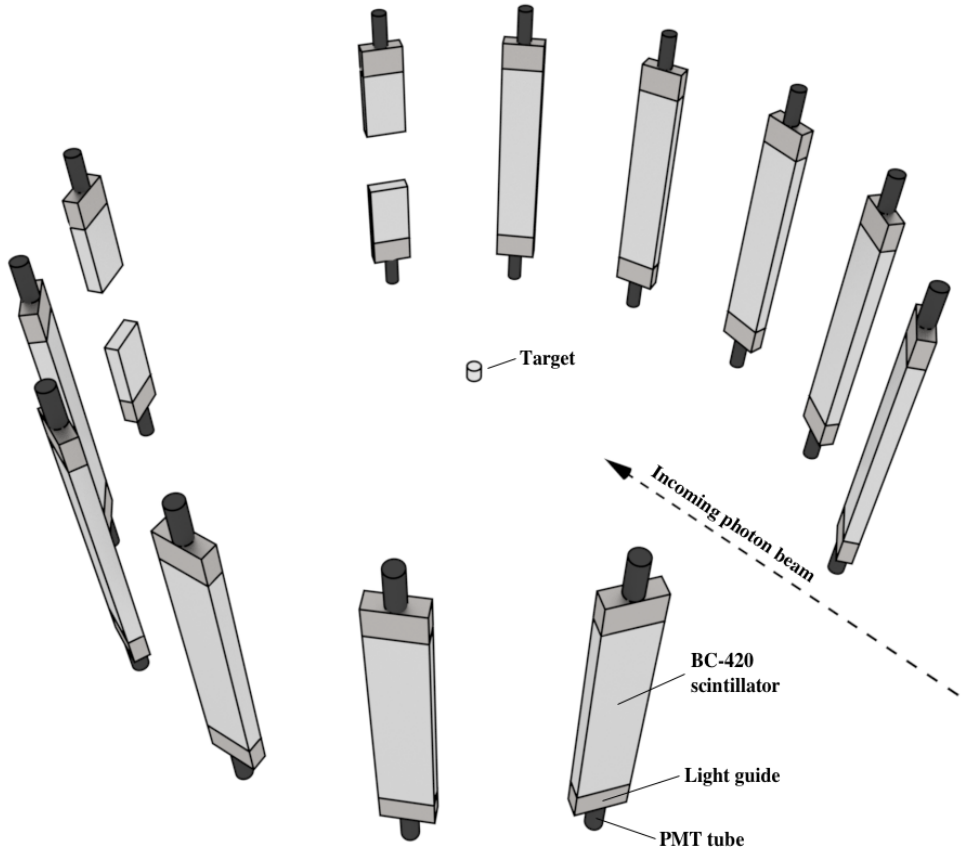

Figure 2.2: 3D-rendering of the bare scintillation cells showing how the detectors are positioned in space. Each detector is fully enclosed in a shielding structure, which is not shown in this depiction.

The neutron detector array consists of fourteen cells made from BC-420 scintillation material acquired from the Transportation Security Administration (TSA) as surplus. The scintillation cells were arranged in a ring around the target (see figure 2.2). Each scintillator is instrumented with two Hamamatsu 580-17 photomultiplier (PMT) tubes, one fixed on each end. In order facilitate the propagation of scintillation light through the scintillators, they were polished to remove micro imperfections and wrapped in reflective Tyvek. Light traveling through the the cell will be reflected back into the cell as a result of

total internal reflection, as long as the cell is free of micro imperfections.

Two different detector designs had to be used in order to address a high rate of gammas on the detectors located furthest downstream of the beam. Ten of the fourteen detectors did not have this problem, and have dimensions of 76.2X15.2X3.8 cm^3. The remaining four had their dimensions reduced to 25.4X15.2X3.8 in order to address particularly rates of gamma detection, which are caused by the scattering of photons from the target. This scattering of photons creates a cone of gammas that engulfs forward facing detectors, leading to very high levels of dead-time and an effective neutron efficiency of zero. To counter this, the two downstream most detectors, at ± 30 degrees from the beam line, were reduced to 1/3 the size of the rest of the detectors and instrumented with only a single PMT. Prior to this modification, the gamma detection rate was nearly 1.0 per pulse in each. After the modification, the gamma detection rate fell to 0.5 gammas per pulse, which lead to a net increase in the effective neutron detection efficiency.

The location of a particle hit along the detector's 30 inch length is determined by the timing difference between signals in the top and bottom PMT . This method uses the fact that the scintillation light travels at a constant speed through the cell. This technique is not possible for the four the downstream detectors at $\pm 30^\circ$, since these have only a single PMT. For these detectors, particle position is assumed to be at the middle of the cell. For further detail on particle position reconstruction, see section 2.2.2.

2.1.2 Data Acquisition

A data acquisition system based on NIM/VME standard was used. A wiring diagram is shown in figure 2.3. The PMTs are supplied voltages ranging from

1300 to 1500 V by a Locroy 1458 high voltage mainframe. The analogue signals from the PMTs are fed into a leading edge discriminator with input thresholds ranging from 30 mV to 50 mV. The logic signals from the discriminator are then converted to ECL logic and fed into a CAEN model V1290A TDC. A gun signal from the accelerator provided the "start" signal for each pulse. On the software side, the acquisition of data from the TDC, along with the conversion of the data into usable formats, was carried out using the CODA software package developed by Jefferson Lab.

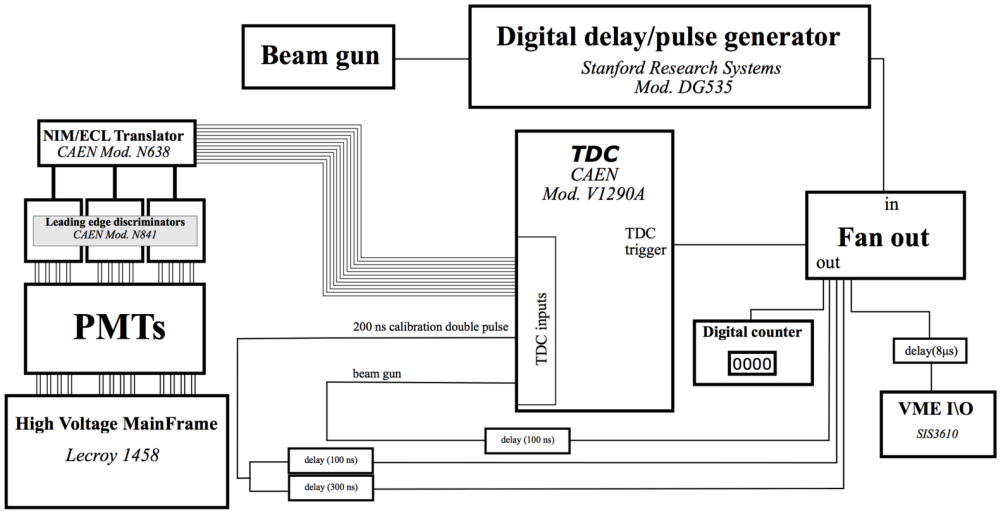

Figure 2.3: Wiring diagram of the entire electronics setup.

2.2 Experimental Methods

2.2.1 Photon Beam

A bremsstrahlung photon beam is produced by the passage of 10.5 MeV electrons through a 1" thick slab of aluminum. Aluminum was chosen for a radiator because it has a neutron knockout threshold above the energy of the electron beam. This ensured that the bremsstrahlung radiator would not be a

source of fast neutrons which would have the potential to make their way into the experimental cell and cause false neutron events. Downstream from the bremsstrahlung radiator, a sweeping magnet removes excess electrons from the photon beam (see figure 2.1). Before reaching the experimental cell, the beam must travel through a series of polyethylene and lead collimators aimed at eliminating beam contaminants. The energy distribution of photons that reach the target was assessed using an MCNP simulation which included the creation and collimation of the bremsstrahlung photons. The resulting energy distribution is shown in figure 2.4.

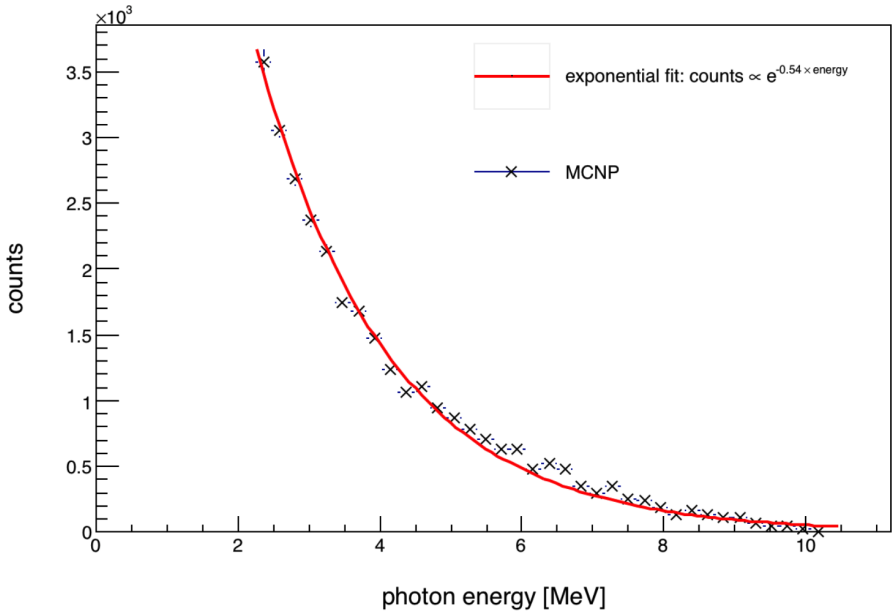

Figure 2.4: Energy distribution of the photons that reach the target, taken from an MCNP simulation of the production and collimation of the Bremsstrahlung beam. The points are from the simulation. The line is an exponential fit of the form Ae^{-bx}. The constant of proportionality, A, is arbitrary. The value for b is 0.54.

When attempting a measurement of prompt neutrons from photofission, an ambiguity can arise between neutrons from photofission and neutrons from (γ, xn). This is because the two reactions have similar cross-sections within

the GDR region. Furthermore, there is significant overlap between the energy spectra of the neutrons from (γ, xn) and those from photofission. Because this measurement is concerned only with observing two neutrons in coincidence, it suffices to set the Bremsstrahlung end-point at 10.5 MeV, since this value is below the target's $(\gamma, 2n)$ threshold of $\sim$12 MeV. Despite setting the end-point below the $(\gamma, 2n)$ threshold, there is still the possibility of detecting multiple neutrons from $(\gamma, 1n)$ in a single pulse, which is referred to as an accidental coincidence. An *accidental* neutron coincidence occurs when two uncorrelated neutrons are detected in the same pulse. The rate of accidentals follow the Poissonian distribution, setting them apart from correlated events, and as a result accidentals can be subtracted from the data. The details and justifications for this procedure are discussed in section 2.3.1.

The electron pulse width was set to 3 ns and had a 1.1A peak current, with a repetition rate of 240 Hz. The 3 ns pulse width is not a large source of error in the measurements of neutron time of flight, since neutron events had a median time of flight of about 80 ns. The accelerator's current is set by requiring that there be, on average, fewer than one fission per pulse in order to diminish the detection of accidentals.

2.2.2 Particle time of flight determination

Each scintillator was equipped with two PMTs, one fixed at each end of the scintillation cell, with the exception of the detectors located farthest downstream at $\pm 30^\circ$ which had a single PMT. The reason for this difference is that, in order to diminish dead-time, the detectors at $\pm 30^\circ$ were segmented to create two independent detectors. Each PMT provides a signal in response to scintillation light with a timing resolution of less than 1 ns, however, the main

source of uncertainly in the time of a particle hit is the variation in the time taken for scintillation light to propagate to the PMTs. The time of events in the PMTs was always taken relative to a signal provided by the accelerator at the beginning of each pulse, referred to as the *beam gun*.

Time of flight (ToF), the time for a particle to travel from the target to the face of a detector, was used to distinguish between photons and neutrons, and to measure neutron energy. The index of refraction in the scintillators is about 3, so there can be up to an 8 ns delay before the light reaches the PMTs as a result of the time required for scintillation light to propagate through the detector. The time of flight was calculated by taking the average between the times of events in the top and bottom PMTs, and then subtracting a calibrated offset. In taking the average, there is a reduction in the sensitivity of the result to the variation of propagate times as a function of the position at which the particle scintillated. This cannot be done in the detectors located at $\pm 30^{\circ}$, because they have only one PMT. However, they are 1/3rd the length of the rest, so scintillation light takes up to 2.5 ns to propagate to the PMT, and this becomes a source of random error in determination of particle position and ToF. See section 2.2.3 for a deeper discussion of experimental errors.

The ToF of a particle causing coincident events in both PMTs of a detector obeys the following relationship:

$$ToF = C_i + \Delta t_{\text{avg}}$$

where Δt_{avg} is the average between the timing from the top and bottom PMTs, and C_i is a constant timing offset which is the same for every pulse. The subscript on C_i is used because the timing offset can be different for each detector.

Any process that produces a timing delay that does not change from pulse to pulse contributes to C_i. Examples of this are the time required for photons to travel from the bremsstrahlung radiator to the target, the propagation of signals through the wires connecting the PMTs, and delays in the electronics for processing.

The time required for scintillation light to travel through the detector, from the point of scintillation to a PMT mounted at either end, can vary from 1 ns for particles that hit very close to a given PMT, to about 8 ns for particles that hit across the detector from a given PMT. The sum of the times taken for scintillation light to travel to the top and bottom PMTs is just the time taken for the light to travel the full length of the detector. The rate at which light propagates along the length of a detector is dependent on speed of light in the material and the light's flight path. The flight paths of detected scintillation light tend to be parallel to the long axis of the detector, because these are the shortest paths possible, and only the first signal from a PMT is accepted. Therefore, in taking the average of the times in the top and bottom PMT, the sensitivity of the result to the varying times required for the propagation of scintillation light is greatly reduced. However, because the scintillation light does not always take to most direct path to a PMT, there is still some variation in the average scintillation propagation times. This variation was measured using a ^{60}Co source, which emits coincident back-to-back photons. The ^{60}Co source is placed at several positions along the face of a lead shielded scintillator. At each position, a small hole is drilled through the lead to give the ^{60}Co source a line-of-sight to a well defined point on the scintillator. A high timing-resolution photon detector is placed next to the ^{60}Co source. When the ^{60}Co source decays, emitting two photons simultaneously, one photon is detected by

the high timing-resolution detector serving as the "start" time, and the other photon scintillates in the detector being calibrated. The times of signals from each PMT, taken relative to the start trigger, are averaged. The photons from ^{60}Co are scintillating at a specified location, so variation remaining in the result is due to varying paths taken by the scintillation light, and is a reflection of the error in ToF measurement. These results can be seen in figures 2.5 and 2.6.

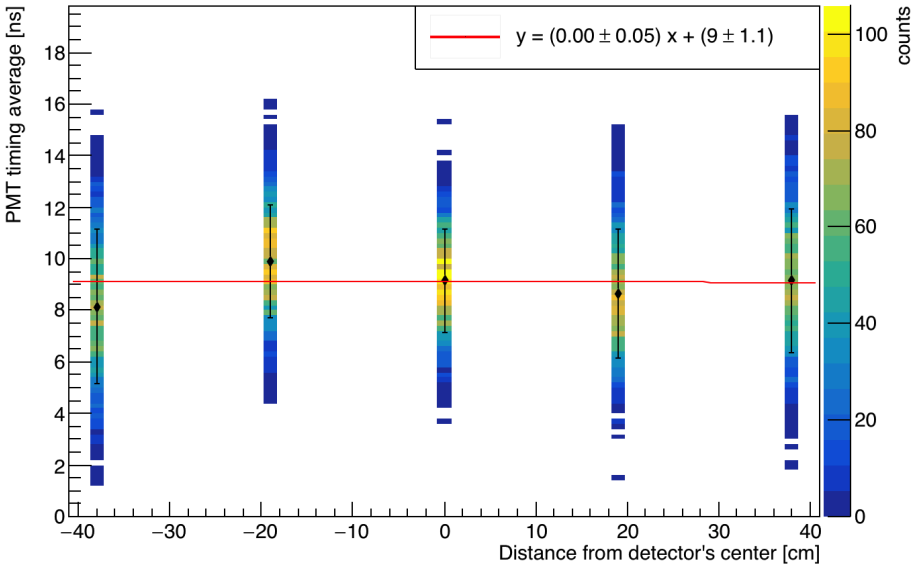

Figure 2.5: A ^{60}Co source, which emits coincident back-to-back photons, is placed at several positions along the face of a lead shielded scintillator. At each position, a small hole is drilled through the lead to give the ^{60}Co source a line-of-sight to a well-defined point on the scintillator. Then, a high timing resolution photon detector is placed close to the ^{60}Co source. When the ^{60}Co source decays, emitting two photons simultaneously, one photon is detected by the high timing-resolution detector serving as the "start" time, and the other scintillates in the detector being calibrated.

The value of the constant offset for ToF calculation is determined by observing photons that scattered from the target. Comparing the timing spectra of a non-neutron producing target made from aluminum, to the spectra produced when no target is used reveals a prominent peak caused by the scattering of photons from the target. These photons must travel between 125 cm to 130 cm to reach

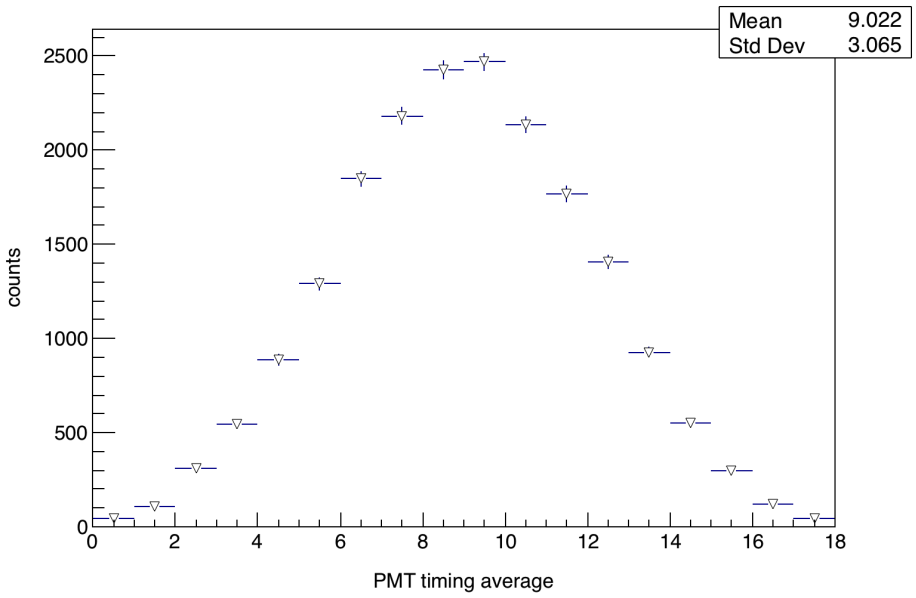

Figure 2.6: Average of times in the top and bottom PMTs. Ideally, scintillation light would always take the same amount of time to travel the length of the detector, producing a delta function in this plot. This is not the case, however, because scintillation light doesn't always take the direct, shortest path to a PMT. Thus, the 3 ns standard deviation of of this curve represents a source of error in the ToF measurement. These data, taken during calibration using a ^{60}Co, are the same data used for fig 2.5, projected onto the y-axis.

a face of a detector, depending on whether the photons reach the detector near the center or at the edge. It takes light 4.0 ns and 4.3 ns to travel 125 cm and 130 cm, respectively. The difference between the two times is negligible for these purposes, so the ToF of photons that scatter from the target is assumed to be 4 ns. With this assumption, the location of the photon peak in the timing spectra can be used to calculate the offset in each detector. See figure 2.7 for an illustration of this process.

2.2.3 Particle Position Reconstruction

Spacial resolution in the horizontal plane is determined by the physical dimensions of the detector. The geometric center of a detector is used for the position, in the horizontal plane, of a particle hit. The detector's dimensions

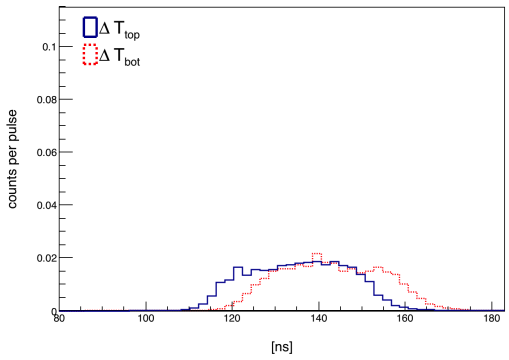

(a) ΔTs with no target in place.

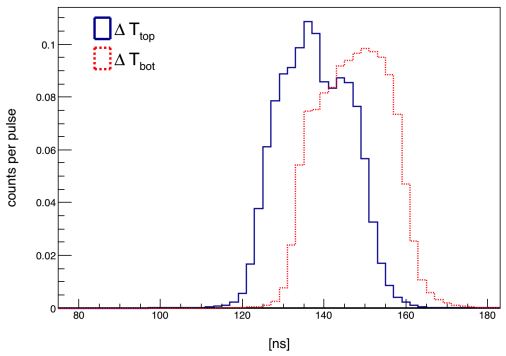

(b) ΔTs with Aluminum target.

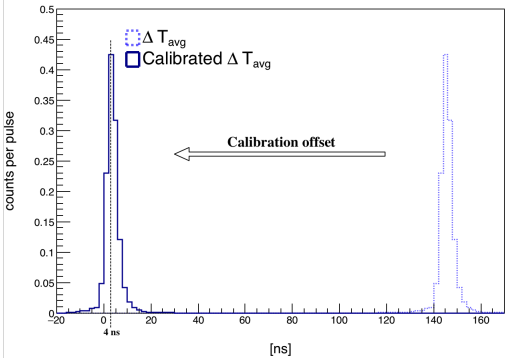

(c) Average of ΔT_{top} and Δt_{bot} with Aluminum target in place.

Figure 2.7: (a) ΔT spectra from each PMT of a detector with no target in place. The beam dump is not able to collect all excess photons, so there is a background despite the lack of a target to scatter photons into the detectors. The background is caused by photons that scatter from various surfaces within the experimental cell. (b) The introduction of a non-neutron producing target made from aluminum produces a peak caused by the scattering of photons from the target. These photons have a constant time of flight, so the width of these spectra are reflective of the range of times taken for scintillation light to propagate from the points of scintillation to a PMT. (c) Taking the average between the ΔTs of the top and bottom PMT gives a sharper peak, since the sum of times from both both PMTs is a reflection of the time required for light to travel the entire length of a detector, regardless of the location of the particle hit. The correct timing offset can be now be found since the photons have a time of flight of 4 ns.

in the horizontal plane are comparatively small at 3.8x15 cm^2, so in doing this, a positional uncertainty of ± 7.5 cm is introduced, which expressed in terms of an angle is $\pm 4^\circ$. The final results of this work use an opening angle bin width of 20°, so $\pm 4^\circ$ is not large enough be a cause for concern. The largest contributor to uncertainty in particle position is the position in vertical direction, which is determined by the timing difference between signals in the top and bottom PMTs.

The determination of a particle's position in the vertical direction relies on the timing of coincident signals from both the PMTs of a detector. The timing difference obeys a linear relationship with respect to the location of the particle hit along the length of the detector. The z-coordinate will hereafter refer to a particle's position along the vertical axis, where $z = 0$ corresponds to the geometric center of the detectors.

As discussed before, detected scintillation light tends to take fairly direct paths to the PMTs, experiencing few reflections off the boundary of the scintillation cell. As a result, the timing difference between signals in the top and bottom PMTs is proportional to the difference in path lengths that the scintillation light must travel to reach each PMT, which is in turn proportional to the z-coordinate of the particle hit. The exact linear relationship is determined through calibration by using collimated photons from a ^{60}Co source. Calibration is achieved by measuring the PMT top-bottom timing difference while the ^{60}Co source is fixed at five different locations along the detectors length. The setup for calibration was discussed in section 2.2.2. The result is shown in figure 2.8.

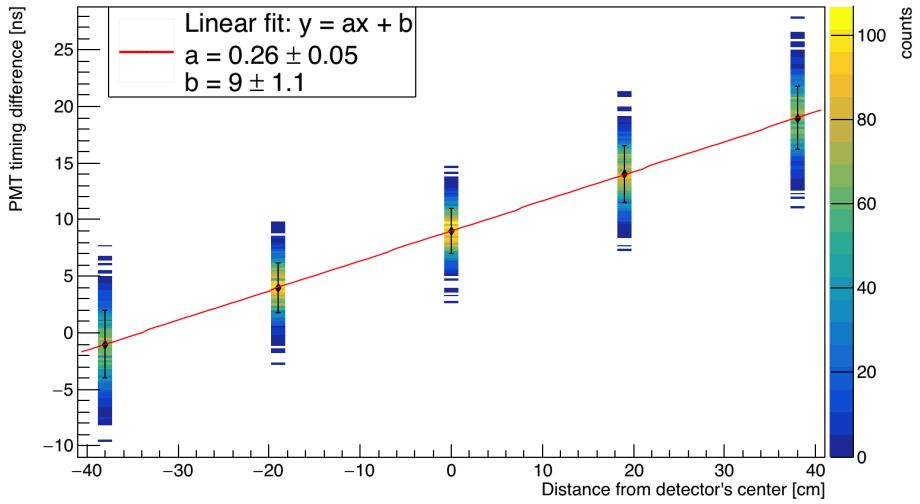

Figure 2.8: A collimated ^{60}Co source is used to produce events at precise locations on the detector. The particle's position along the detector's length is shown to vary linearly with respect to the timing difference between events in the top and bottom PMTs of a detector.

Discussion of Experimental Errors

ToDo.

Detector Shielding

The detector's shielding was designed with the aim of reducing cross-talk, the detection of photons, and noise. The front face of the detectors, which face towards the target, are subject to the highest flux of gammas due to the scatting beam photons from the target. The detection of a gamma renders a detector "dead" during the time in which fission neutrons reach the detectors. Lead readily attenuates gammas, but has the side effect scattering neutrons. If a neutron scatters prior to being detected, the ToF calculation will be incorrect because the neutron traveled an unknown distance to the detector. The extent to which neutron distances of travel are perturbed due to scattering from lead shielding was quantified using an MCNP . Accordingly, 1" of lead was placed along the front face of the detectors. This effectively diminished gamma de-

tection rates and, according to the simulation, is expected to cause negligible levels of neutron scattering. Additional lead was used in some special areas that had high gamma flux: at the sides of detectors adjacent to the beam, and along the front faces of the detectors farthest downstream.

Placing lead behind the detectors was avoided in consideration of an MCNP-POLIMI simulation, which indicated that lead placed here facilitates cross-talk. *Cross-talk* is an undesirable phenomenon in which a particle causes a hit in one detector, and then by any means (e.g. scattering), the same particle causes a hit in a different detector. If both hits occur within the time frame typical for neutrons, then the cross-talk event cannot be distinguished from a true neutron coincidence. Because cross-talk events are in fact correlated, they cannot be removed in analysis by the subtraction of accidentals.

2.2.4 Detector Cross-talk

The geometry of the neutron detector array makes it kinematically impossible for a neutron to scatter from a proton in one detector–which is the basis for scintillation–then travel directly to another detector. Rather, it is kinematically required that the neutron scatter from at least one intermediate nucleus while traveling between detectors. This fact, which can be derived from simple two-body kinematics, means that cross-talk is a "second-order" effect, because upon depositing enough energy to be detected in one scintillator, the neutron must then 1) scatter from an intermediate nucleus, and 2) be detected in a second detector. The fact that crosstalk is a second order effect is not sufficient to make the claim that cross-talk is negligible, however, because the detectors and their shielding contain significant levels of carbon, lead, and other nuclei which could function as intermediate scattering points. To address this, a

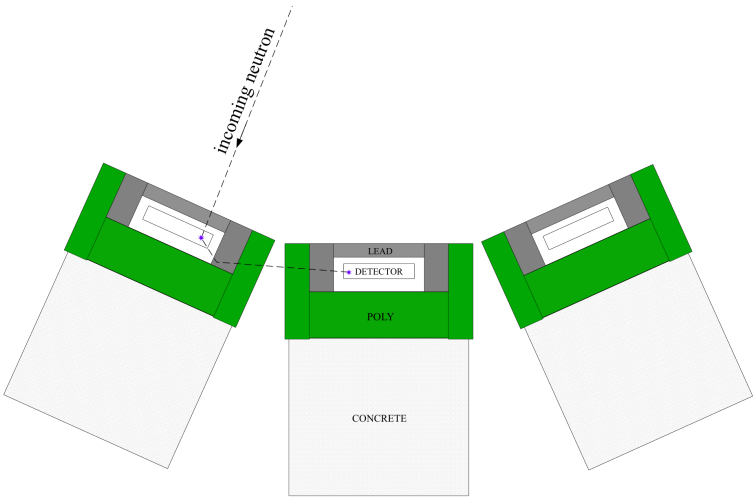

Figure 2.9: An example of a neutron cross-talk event. First, an incoming neutron enters a detector and is detected because of a collision with a proton. Next, it scatters from lead shielding nearby, changing its direction of travel such that it enters a second detector, where the neutron is detected a second time. The scattering of a neutron from an intermediate nucleus, in this case a Pb nucleus in the detector's shielding, is kinematically required in order for cross-talk to occur.

detailed MCNP-PoliMi simulation was performed that modeles the entire neutron detector array, shielding, supporting structures, and the experimental cell. PoliMi is an extension to MCNP that was developed to simulate correlated particles and their subsequent interactions as accurately as possible. PoliMi includes multiplicity distributions for neutrons, photons, and the correct correlated photon production from neutron interactions. These features are in contrast to the standard release of MCNP which uses uncorrelated distributions and average multiplicities. In doing so, the standard release of MCNP converges to the correct average result quicker than if correlated event-by-event distributions were used. Another feature PoliMi provides is the ability for particle tracking to be printed and post processed by the user. Here, the particle tracking data is used to model detector physics in order to estimate the experimental rate of neutron cross-talk as it compares to true neutron coincidence.

Neutron detection physics was modeled by converting the amount of energy deposited by neutrons into scintillation light output, but did not include the propagation or detection of scintillation light. The scintillation light output is given in MeV equivalent electron energy, denoted MeVee. Neutron energy deposit during collisions with protons and carbon is the input to the algorithm used to calculate light output, the procedures of which are taken from ref **??**. For neutrons detected by elastic scattering on hydrogen, the light output is given by

$$L = 0.0364E_n^2 + 0.125E_n$$

, where E_n is the energy deposited by the neutron, equal to the change in kinetic energy. Neutron interactions with carbon are assumed to generate a small light output equal to

$$L = 0.02E_n$$

The simulation used a ^{252}Cf spontaneous fission source built-in to MCNP-POLIMI which emits neutrons with the correct correlations. The light output threshold for particle detection was set empirically by picking a light output that gives good agreement between the ToF spectra of simulation and experiment (see fig 2.10). While tracking through each particle history, a tally is kept of number of cross-talk events and the number of correlated neutron pairs detected. An event is considered a ”neutron event” if a particle produces ¿=[find!] MeVee of light output in a detector at any time within the neutron time of flight range used in the experiment, which was 45 to 150 ns. In doing so, the method for particle identification in the simulation mimics that which is used in the experiment. The relative amount of cross-talk is quantified by taking the ratio between the number of cross-talk events and the number of

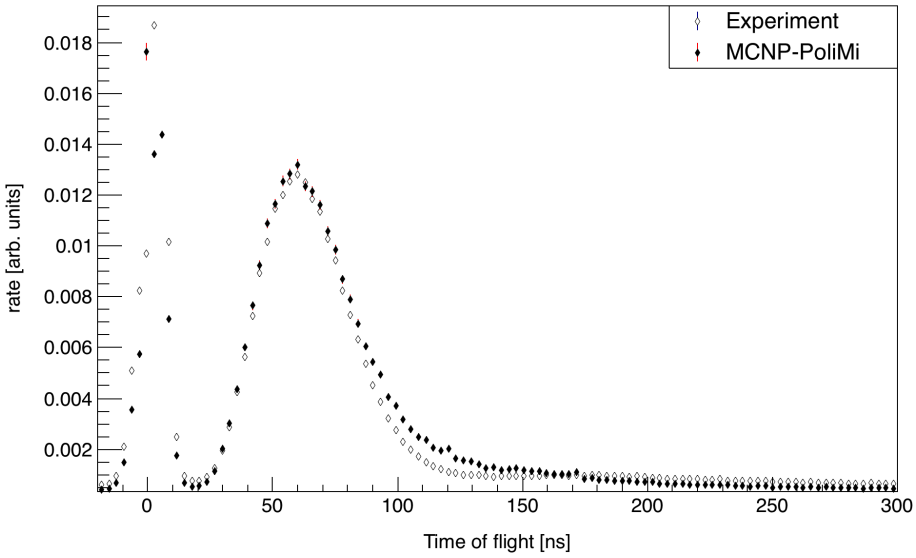

Figure 2.10: ToF spectra of ^{252}Cf from experiment vs MCNP-PoliMi. The simulation modeled the detector setup and detector response.

correlated events. Cross-talk events occurred in the simulation at a rate that is 3% the rate of correlated events. Accordingly, no cross-talk corrections were applied to the data.

2.2.5 Targets

A depleted uranium (DU) target with dimensions of 4x2x0.05 cm^3 was used as the primary target for the measurement of two-neutron correlations. DU received the majority of the allotted beam time because it is an even-even nucleus, and as a consequence the fission fragments are emitted with a high degree of anisotropy. One consideration for the design of the target is the rate at which neutrons produced in the target scatter before exiting the target. This is a cause for concern because a neutron's direction of the travel is altered by scattering, which creates two-neutron opening angles that are not reflective of the opening angle immediately after fission. This effect cannot be completely eliminated, so the target must be small enough such that neutron scattering is

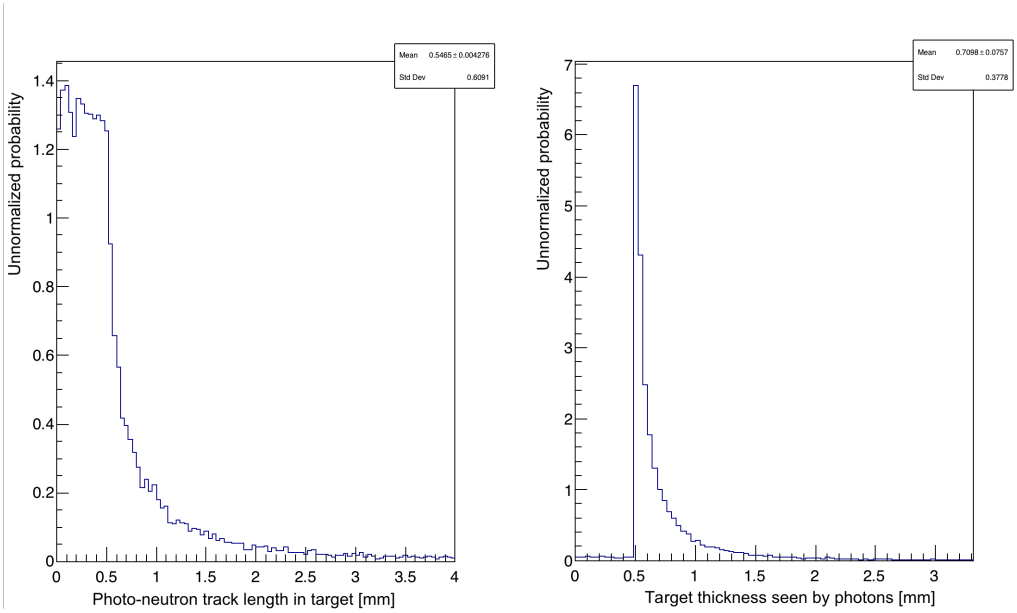

Figure 2.11

negligible. The size of such a target is found by performing an MCNP simulation in which neutrons with an energy spectrum typical of fission neutrons are sampled uniformly within the target. From the simulation, 97.5% of the neutrons produced in a 4x2x0.05 cm^3 DU target escaped without scattering. Because two neutrons are required for the formation of an opening angle, the rate of data contamination due to scattering would be $(1 - .975^2)$, or 5% of two-neutron events.

It is desirable to have a target with symmetry that is consistent with the cylindrical symmetry of the neutron detector array. To accomplish this, a thin rectangular target was rotated slowly about the vertical axis during data acquisition. By doing this the cylindrical symmetry is preserved, since the measurement is reflective of an average of events which occurred while the target was at orientations from 0 to 2π. This eliminates potential biases caused not by physics, but instead by the asymmetrical structure of the target.

2.2.6 Measurements with ^{252}Cf

Opening angle measurements were also performed on neutrons from the spontaneous fission (SF) of ^{252}Cf. The configuration for this was different than that for photofission measurements, as the photon beam can no longer be used for the timing of a "start" trigger. The trigger for ^{252}Cf consisted of two high timing-resolution scintillation photon detectors, where one is fixed below and the other above the source at a distance of 15 cm. Using a coincidence window of 4 ns, the timing start trigger required 2-fold coincidence between both the photon detectors. Aside from a different mechanism for a start trigger, the methods used for the measurement of two-neutron opening angle distributions in the SF of ^{252}Cf are equivalent to those used for photofission.

As opposed to the measurements of neutrons from photofission, there is no concern over the detection of accidental neutron pairs because given the strength of the ^{252}Cf source, it is highly unlikely for two fissions to occur during the neutron time of flight window. Another difference between the two measurements is the clean and sharp peak produced by fission photons from ^{252}Cf, compared to a relatively smeared peak produced by photons scattering from the target during measurements of photo-neutrons. In each measurement, the photon peak is used as a reference point for the calculation of neutron ToF. As a result the ^{252}Cf measurements have less error in ToF caused by the spreading of the photon peak used for reference. The same normalization technique is used for both measurements, in which the correlated distribution is divided by the uncorrelated distribution of neutron pairs taken from different fissions. There is good agreement among past measurements of the opening angle distribution of neutrons from the spontaneous fission of ^{252}Cf, and so they serve as a good benchmark for the quality of measurements performed in this study.

2.3 Data Analysis

The efficiency and acceptance of the neutron detector array varies greatly over the range of opening angles from 0 to 2π (see figure 2.12a). This effect is due to the detector array's non-spherical symmetry, and to varying efficiency as a function of particle position. There was no attempt to measure the array's efficiency as a function of two-neutron opening angle, because it is not necessary and would have been a difficult task. In this experiment, angular correlation is calculated by normalizing each measurement to an equivalent distribution of uncorrelated neutrons, giving a result that is insensitive to detector efficiencies (see figure 2.12b). The equivalent uncorrelated distribution is formed from a set of manufactured two-neutron events, in which each neutron is taken from a different pulse. The opening angles between the neutrons are then calculated as normal. Such pairs will hereafter be referred to as different pulse (DP) pairs. The neutrons of a DP pair are uncorrelated because events in one pulse do not have casual influence on the events in another pulse. Detector efficiency and geometry influence same pulse (SP) events and different pulse events equally. Thus, barring two-neutron correlations and a scaling factor, the DP distribution is identical to the SP distribution. Each pair of pulses is chosen such that the two pulses occurred within less than a few 100 ms of each other. This ensures that both pulses are subject to the same experimental conditions, thereby lessening systematic effects from time varying factors such as high-voltage drift and varying beam current. As many pairs as needed can be readily selected until good counting statistics is achieved, because the only restriction for selecting pulse pairs is that they occurred around roughly the same time.

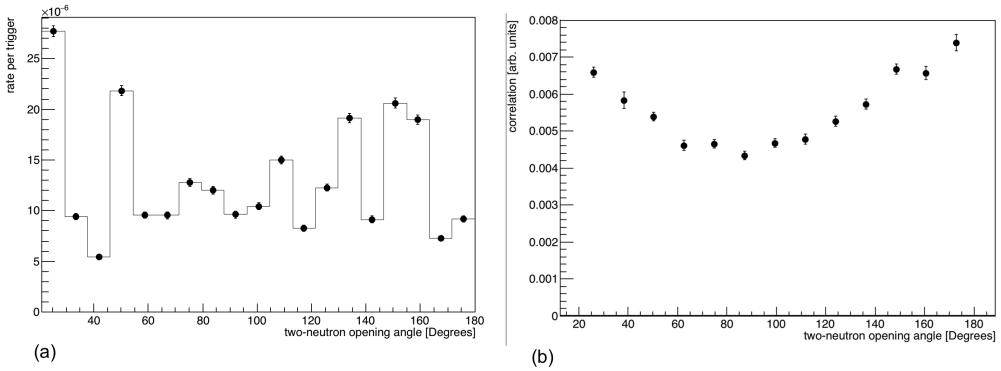

Figure 2.12: (a) Unnormalized two-neutron opening angle distribution from the spontaneous fission of ^{252}Cf. The structure is reflective of geometric acceptance and efficiencies. (b) Same distribution after division by uncorrelated two-neutron events, which are taken from different pulses.

2.3.1 Subtraction of Accidentals

An accidental neutron coincidence is defined as a coincidence between two uncorrelated events in a single pulse. For example, a coincidence between a neutron from a (gamma,1n) reaction and a neutron from photofission. Another example is a coincidence between two events that are part of the noise background. In both of these examples, the two events are considered accidentals because they have no causal influence on each another. A true neutron coincidence, or true for short, is defined here as any pair correlated neutrons from the same pulse.

Accidentals are removed from the data by subtracting 1/2 times the equivalent distribution formed by the DP data. The factor of 1/2 arises from the Poissonian statistics that inherently govern all accidentals, whether the accidental events are composed of two neutrons, two photons, two noise events, or any combination thereof. An accidental is comprised of the occurrence of two independent events. Therefore, as per Poissonian statistics, the probability of

measuring an accidental in a single pulse is given by:

$$SP_{\mathrm{a}} = \frac{e^{-\lambda}\lambda^2}{2} \approx \frac{1}{2}\lambda^2$$

where SP_a is the accidental rate of single pulses, λ is the mean accidental rate of single pulses–an unknown value. In this study, the coincidence rates were around 5×10^{-5} events per pulse, so the approximation used above is correct to within 0.001% as the worst case scenario. Since the DP data is formed by observations of events from two different pulses, the DP accidental rate is equal to the Poissonian probability of one event, squared.

$$DP_{\mathrm{a}} = (e^{-\lambda}\lambda)^2 \approx \lambda^2$$

where DP_{a} is the accidental rate of DP events. Therefore, if coincidence rates, then the rate of measured accidentals in single pulses is $1/2$ times the rate of accidentals in the different pulses. In this study the subtraction had about a ten percent effect.

Chapter 3

Results

Chapter 4

Concluding Remarks

In summary, we have reported on the first ever measurement of two-neutron opening angle distributions from the photofission of ^{238}U, and their dependence on mean neutron energy. Photofission was achieved by means of a Bremsstrahlung photon beam produced by the passage of 10.5 MeV electrons through a 1" thick slab of Aluminum. Electrons were produced by a 44 MeV capable, low duty factor, pulsed linear accelerator housed at the Idaho Accelerator Center.

By virtue of performing a measurement of pairs of correlated fission neutrons, an equivalent distribution of uncorrelated neutron pairs was able be constructed, which served as a normalizing distribution. By normalizing measurements to this distribution, the dependence of the measurement on detector efficiencies and geometry was eliminated.

Appendix A

Dummy Appendix

ToDo: put some MCNP decks here, just because.

Bibliography

[1] Harry R. Bowman, Stanley G. Thompson, J. C. D. Milton, and Wladyslaw J. Swiatecki. Velocity and angular distributions of prompt neutrons from spontaneous fission of cf^{252}. *Phys. Rev.*, 126:2120–2136, Jun 1962.

[2] C. Budtz-JÃžrgensen and H.-H. Knitter. Simultaneous investigation of fission fragments and neutrons in 252cf (sf). *Nuclear Physics A*, 490(2):307 – 328, 1988.

[3] J. T. Caldwell, E. J. Dowdy, R. A. Alvarez, B. L. Berman, and P. Meyer. Experimental determination of photofission neutron multiplicities for 235u, 236u, 238u, and 232th using monoenergetic photons. *Nuclear Science and Engineering*, 73(2):153–163, 1980.

[4] S. Debenedetti, J. E. Francis, W. M. Preston, and T. W. Bonner. Angular dependence of coincidences between fission neutrons. *Phys. Rev.*, 74:1645–1650, Dec 1948.

[5] A. M. Gagarski, I. S. Guseva, V. E. Sokolov, G. V. Val'Ski, G. A. Petrov, D. O. Krinitsin, D. V. Nikolaev, T. A. Zavarukhina, and V. I. Petrova. Neutron-neutron angular correlations in spontaneous fission of 252Cf. *Bulletin of the Russian Academy of Sciences, Physics*, 72:773–777, July 2008.

[6] N.V Kornilov, A.B Kagalenko, S.V Poupko, P.A Androsenko, and F.-J Hambsch. New evidence of an intense scission neutron source in the 252cf spontaneous fission. *Nuclear Physics A*, 686(1):187 – 203, 2001.

[7] G. A. Petrov. Current status of the search for scission neutrons in fission and estimation of their main characteristics. *AIP Conference Proceedings*, 798(1):205–212, 2005.

[8] Sara A. Pozzi, Brian Wieger, Andreas Enqvist, Shaun D. Clarke, Marek Flaska, Matthew Marcath, Edward Larsen, Robert C. Haight, and Enrico Padovani. Correlated neutron emissions from 252cf. *Nuclear Science and Engineering*, 178(2):250–260, 2014.

[9] J. S. Pringle and F. D. Brooks. Angular correlation of neutrons from spontaneous fission of ^{252}Cf. *Phys. Rev. Lett.*, 35:1563–1566, Dec 1975.

[10] C. P. Sargent, W. Bertozzi, P. T. Demos, J. L. Matthews, and W. Turchinetz. Prompt neutrons from thorium photofission. *Phys. Rev.*, 137:B89–B101, Jan 1965.

[11] Seregina. *Measurements and Analysis of Angular-Energy Distribution for 252Cf (SF) neutrons*. PhD thesis, IPPE, Obninsk, Russia, 1985.

[12] Olivier Serot, Olivier Litaize, and Abdelaziz Chebboubi. Influence of scission neutrons on the prompt fission neutron spectrum calculations. In *EPJ Web of Conferences*, volume 146, page 04027. EDP Sciences, 2017.

[13] V. E. Sokolov and G. A. Petrov. Investigation of the angular dependences of neutron-neutron coincidences from 252cf, 235u, 233u and 239pu fission in search of scission neutrons. *Proc. XVIII Internat. Seminar on Interaction of Neutrons with Nuclei (ISSIN-18)*, pages 108–118, 2010.